

Modeling the adaptive optics systems on the Giant Magellan Telescope

Marcos A. van Dam,^a Philip M. Hinz,^b Johanan L. Codona,^b Michael Hart,^b Aurea Garcia-Rissmann,^b Matt W. Johns,^c Stephen A. Slichtman,^c Antonin H. Bouchez,^c Brian A. McLeod^d and Francois Rigaut^e

^aFlat Wavefronts, P.O. Box 1060, Christchurch 8140, New Zealand;

^bSteward Observatory, University of Arizona, 933 North Cherry Avenue, Tucson, AZ 85721, USA;

^cCarnegie Observatories, 813 Santa Barbara St., Pasadena CA 91101, USA;

^dHarvard-Smithsonian Center for Astrophysics, 60 Garden Street, Cambridge, MA 02138, USA;

^eGemini Observatory, c/o AURA, Casilla 603 La Serena, Chile

ABSTRACT

Modeling adaptive optics (AO) systems is crucial to understanding their performance and a key aid in their design. The Giant Magellan Telescope (GMT) is planning three AO modes at first light: natural guide star AO, ground-layer AO and laser tomography AO. This paper describes how a modified version of YAO, an open-source general-purpose AO simulation tool written in Yorick, is used to simulate the GMT AO modes. The simulation tool was used to determine the piston segment error for the GMT. In addition, we present a comparison of different turbulence simulation approaches.

Keywords: Adaptive optics, Giant Magellan telescope, simulations, wavefront sensing

1. INTRODUCTION

Adaptive optics (AO) has found widespread use in astronomical settings to compensate for atmospheric turbulence and telescope aberrations. All of the current generation of 8-10 m telescopes are equipped with AO. Studies are under way to design the AO systems for the next generation of telescopes: the Thirty Meter Telescope (TMT), the European Extremely Large Telescope (E-ELT) and the Giant Magellan Telescope (GMT). A key tool in the design of these AO systems is the ability to simulate their performance. Le Louarn *et al* summarizes the state-of-the-art in AO simulations.¹

The AO program at GMT is described in Hinz *et al.*² The baseline design of the GMT AO system calls for three first-light AO modes, all of which use the adaptive secondary deformable mirror (DM), conjugate to a height of 200 m above the ground, as the only corrective element. The first mode is the classical natural guide star (NGS) mode, where a single NGS is used to correct the wavefront in the direction of the guide star. The second mode is ground-layer adaptive optics (GLAO), where a number of laser guide stars (LGSs) are used to sense the high-order wavefront complemented by low-order wavefront measurements from one or more NGSs. The DM corrects the low altitude component of the wavefront to improve the seeing over a large field of view. Finally, laser tomography adaptive optics (LTAO) has a similar guide star configuration to GLAO, but laser tomography is used to estimate the three-dimensional structure of the atmospheric turbulence, which is corrected by summing the contribution of these atmospheric layers along the optical axis. Another related concept which we intend to study is the performance and sky coverage improvement gained by using the tomographic wavefront reconstruction to sharpen, in open loop, the tip-tilt star sensed at infrared wavelengths.

This paper and another³ outline the progress made in modeling the GMT AO system using end-to-end simulation tools, and the lessons learned along the journey. The aim of the simulation effort is two-fold: to

Further author information: send correspondence to Marcos van Dam, marcos@flatwavefronts.com

produce performance predictions for the different modes of the AO systems, and to aid in making design decisions and exploring parameter space.

The initial simulation effort used WaveTrain, a commercial software package developed by MZA Associates Corporation. However, significant limitations to the software were encountered when attempting to tailor the simulations to the GMT case, since it was very difficult to adapt the code for our purpose. Consequently, it was decided to pursue two other avenues in parallel to reduce the risk of running into another dead-end.

The first approach was to create a custom simulation tool written in Matlab specifically for the GMT, called AOSim2 and described in Knox *et al.*³ Writing our own code has the obvious advantage that all the necessary features are included by design. The drawback is that AOSim2 is, at least in the short term, feature deficient with respect to more established codes.

The second approach was to determine whether an existing code could be modified to meet the needs of GMT. After a broad survey of existing AO simulation codes, YAO, an open-source, general-purpose AO simulation tool written in Yorick by Francois Rigaut, was selected.⁴ The advantages of YAO are its comprehensive feature set, the ease with which modifications can be made and the support available from its author. YAO simulations are controlled by a parameter file that contains a number of different data structures. Each data structure has information about one of the following: simulation dimensions, telescope pupil, atmospheric turbulence, guide stars, WFSs, DMs, reconstructor, control law, science targets and simulation iterations. After these parameters are loaded, the simulation is initialized (by creating the appropriate influence and reconstruction matrices, *etc*) and then a number of iterations of the simulation are run. The important modifications made to the code are documented in Section 2. Section 3 describes the implementation of the various AO modes. Section 4 presents some related results: an estimate of the segment piston error for the GMT running in NGS AO mode and a comparison of various turbulence simulation codes. Finally, concluding thoughts are presented in Section 5.

2. MODIFICATIONS TO YAO

In this section, we report on the important upgrades and modifications made to YAO for our purposes. The latest available version, YAO 4.5.0 running in Yorick 2.1.05x, was used. This version has support for pupils, wavefront sensors and DMs that are user-defined.

2.1 GMT pupil

The GMT pupil consists of seven round segments: a central segment surrounded by six outer segments in a petal configuration. The segments are 8.4 m diameter, with the outer ring of segments centered at a distance of 8.7 m from the center of the telescope. The center segment's obstruction is 3.1 m in diameter and modeled as a circle. The gap between segments is sufficiently large that the wavefront discontinuities between the segments present a real challenge to AO design. Initially, we simulated the system by implementing seven separate WFSs and DMs and an additional segment piston WFS and segment piston DM to phase the disjoint DMs in order cancel atmospheric segment piston. However, the structure of YAO, with a single reconstructor matrix and a vector-matrix multiply to perform the wavefront reconstruction, means that treating the problem as seven separate AO systems does not lead to any reduction in computation. The simulations reported here bundle all the DM actuators together regardless of what segment they correspond to, and similarly for the WFS subapertures from a given guide star. However, the inclusion of a piston WFS, described in Section 2.2, is still needed to optimally phase the segments.

2.2 Piston wavefront sensor and deformable mirror

An important problem for GMT is how to sense the differential piston between the segments. There is currently no consensus on what technique will be used to accomplish this. A perfect piston WFS was implemented in YAO which measures the mean wavefront at each segment and uses this measurement to drive a fictitious piston DM. In this way, we can create simulations that are not affected by segment piston error, and also estimate the residual segment piston error as a function of the frame rate of the piston WFS.

2.3 Wavefront reconstruction

In the remainder of this paper, we assume that Shack-Hartmann WFSs are used to estimate the atmospheric turbulence. These sensors estimate the wavefront slope at several locations in the pupil by measuring the centroid of subimages of the pupil. The process of converting from measured wavefront slopes (or centroids) to a wavefront estimate is called wavefront reconstruction. In classical AO systems, the centroids are multiplied by a reconstruction matrix to produce an estimate of the residual wavefront. There are several competing approaches to compute the reconstruction matrix, the most general of which is the truncated singular value decomposition (SVD). This is the only reconstructor implemented in the released version of YAO. While SVD reconstructors work well for AO systems with a modest numbers of actuators, they are very burdensome to compute and result in extremely poor performance for the GMT NGS AO system. Consequently, we implemented regularized least-squares reconstructors, which take the form:

$$R = (G^T G + \alpha A^T A)^{-1} G^T, \quad (1)$$

where G is the influence matrix (also known as the poke matrix) and α is a positive scalar parameter that determines how much weight to put on the regularization term, $A^T A$. A simple choice that worked well in the simulations was to set $A^T A$ to the identity matrix, I . Other good choices for the regularization term are inverse covariance matrix for Kolmogorov turbulence, C_ϕ^{-1} ,⁵ or $L^T L$, where L is the Laplacian operator.^{6,7}

For AO systems with a very large number of actuators and centroid measurements, the interaction matrix is usually sparse because every actuator on the DM only affects the centroids in neighbouring subapertures. A sparse A matrix can be selected at a minimal cost in performance by ignoring the correlation effects between actuators that are not close to each other.⁷ It is more computationally efficient to use sparse matrix techniques to compute the residual wavefront. SOY, a plugin for Yorick (also available for IDL) developed by Ralf Flicker,⁸ can be used to take advantage of the sparse nature of these matrices.

The residual wavefront is calculated in two steps. First, multiply the centroids, s , by the transpose of the poke matrix to give a vector, b :

$$b = G^T s \quad (2)$$

and then use a preconditioned conjugate gradient method with a suitable starting estimate to solve for the residual wavefront, c :

$$(G^T G + \alpha A^T A)c = b. \quad (3)$$

The term $G^T G + \alpha A^T A$ is only computed once (although it can easily be updated on the fly), while the reconstruction matrix is never explicitly calculated.

The options to use a regularized least-squares reconstructor or to bypass the reconstructor matrix and compute the residual wavefront using the sparse matrix techniques is controlled by setting a parameter in the YAO parameter file.

2.4 Open loop control

Open loop control implies that the WFSs measure the wavefront before it is corrected by the DM. With rare exceptions,⁹ existing AO systems operate in closed loop. However, AO concepts are being pursued which will operate partly or completely in open loop. We have modified YAO to allow the WFSs to operate in an open loop configuration.

2.5 Other limitations

While YAO has a very extensive feature set, there are some limitations of the software for our purposes.

In YAO, the sodium structure with altitude is assumed to be a Gaussian distribution specified by two parameters: sodium elevation and sodium thickness. Due to the finite thickness, elongated spots are produced on the WFS and these are modeled by convolving the WFS image from a point source by the effect of the spot elongation experienced by each subaperture. This approach is adequate to simulate measurement noise; however, this does not model the focus and LGS aberrations induced by the change in the sodium layer height and structure.¹⁰ We will model these effects separately with dedicated code, rather than including it in YAO.

LTAO requires the use of tomographic reconstructors to reconstruct the 3-D structure of turbulence. A description of the implementation under consideration is described in Section 3.3.

Finally, YAO does not yet parallelize any tasks. There is an effort underway to make YAO use all the processors that are available, which will greatly reduce simulation time on multi-core machines.

3. IMPLEMENTATION OF SIMULATIONS IN YAO

In this section, we describe how the various AO modes are implemented in YAO. The goal was to demonstrate our ability to carry out these simulations, and to identify any stumbling blocks, such as feature deficiencies and the limitations of memory and CPU on a PC. AO performance results and the exploration of parameter space are beyond the scope of this paper.

3.1 NGS simulations

The existing design for the GMT NGS system uses a Shack-Hartmann WFS: other wavefront sensing concepts will be investigated in the near future.

A basic, proof-of-concept simulation was run with the following parameters:

- 250x250 pixels in total
- 50x50, 0.516 m subapertures with 5x5 pixels per subaperture in the pupil plane
- 2x2 0.5" pixels per subapertures in the image plane
- $r_0=0.2$ m at 650 nm and a sensing wavelength of 650 nm
- A DM and a tip-tilt mirror guiding on a single NGS
- A segment piston DM guiding on a segment piston WFS

The small number of pixels per subaperture was chosen to enable the simulations to be set up and run quickly. Note that 5x5 pixels per subaperture are not really sufficient for three reasons. First, to avoid problems with phase wrapping, there should be at least three pixels per r_0 at the wavefront sensing wavelength. The coherence length at 650 nm is only 0.274 m, so there are only 2.7 pixels per r_0 . Second, having 5x5 pixels limits the field-of-view of the wavefront sensor to

$$\begin{aligned} FOV &= 206265 \times 650 \times 10^{-9} \times 5/0.512 \\ &= 1.31'' \end{aligned} \tag{4}$$

so each pixel in the quad cell can be no greater than 0.65". Third, the DM fitting error is underestimated when there are only 5x5 pixels per subaperture.

The simulation speed when using a Dell Inspiron 15 Laptop with a 32-bit Intel Celeron Dual Core 1.83 GHz Processor running Linux is tabulated in Table 1. The simulation time could be reduced by not estimating the target PSFs and also by using a geometric method to do the wavefront sensing rather than generating the Shack-Hartmann spots and calculating their displacement.

3.2 GLAO simulations

The aim of GLAO is not to produce near diffraction-limited images but to produce seeing-limited images with a reduced seeing disk by eliminating the contribution from the low altitude turbulent layers. It is important for the AO correction to be uniform across the whole field of view when using GLAO. While a tomographic wavefront reconstruction can lead to better image quality near the center of the image, it has been shown that the optimal uniformity of PSF are obtained by placing the laser guide stars in a circular beam centred around the center of the field to be imaged and taking the average of the wavefront sensors.¹¹ Indeed, this is what is implemented in most GLAO simulations.¹² The baseline design for the GMT GLAO module calls for six sodium LGSs, all at

Process	Time (ms)
WF sensing	89.78
Reset and measurement history handling	0.16
Vector-Matrix multiplication	38.95
DM shape computation	45.31
Target PSFs estimation	55.71
Displays	13.65
Circular buffers, end-of-loop printouts	0.05
Iterations per second	4.098

Table 1: Time taken to run the NGS AO simulations for the GMT case.

the same radius from the center, and one or more NGSs. The reconstruction matrix is then computed as the regularized least-squares inverse of the poke matrix, which is created by poking the actuators on the DM and measuring the centroid on the six high-order WFSs. The tip-tilt is reconstructed and compensated separately, guiding on the NGS and correcting with a dedicated tip-tilt mirror.

The simulation parameters that differ from the NGS case are:

- 2x2 2.0" pixels per subapertures in the image plane
- $r_0=0.2$ m at 500 nm and a sensing wavelength of 2600 nm
- A DM guiding on six LGSs and a tip-tilt mirror guiding on a single NGS

Note that the sensing wavelength was set artificially high to increase the field-of-view of the WFS to accommodate the elongated LGS spots. This can be avoided by having more pixels, as discussed in Section 3.1.

The compute time for the GLAO case is tabulated in Table 2. The computational time could be reduced by adding the centroids together before multiplying by a reconstructor much reduced in size.

Process	Time (ms)
WF sensing	568.00
Reset and measurement history handling	0.75
Vector-Matrix multiplication	229.71
DM shape computation	38.70
Target PSFs estimation	176.98
Displays	44.62
Circular buffers, end-of-loop printouts	4.23
Iterations per second	0.940

Table 2: Time taken to run the GLAO simulations for the GMT case.

Since GLAO is effectively a way to reduce the effect of the seeing, and the seeing is aperture independent for telescopes much larger than Fried's parameter, it is possible to carry out certain GLAO trade studies quickly by using a smaller telescope aperture. The only difference is that larger telescopes will obtain more benefit from a finite outer scale, with or without GLAO correction, and this has to be taken into account.

3.3 LTAO simulations

LTAO systems are a special case of multi-conjugate adaptive optics (MCAO), where there is only one DM. The wavefront reconstruction for MCAO consists of two steps: estimating the turbulence in 2.5-D (where a 2-D estimation of the turbulence is made over a modest number of representative turbulence layers) followed by a fit of the turbulence to the DMs.^{7, 13, 14}

The estimation step relies on knowing the location of the DM actuators, since this affects the centroid measurements. Early simulations avoided this problem by running the simulations in open loop, where the DM commands do not affect the WFS.^{7,13,14} Later work extended this approach to closed-loop operation: pseudo-open loop control uses the existing actuator commands as well as the centroids to determine the residual wavefront.¹⁵ It is suboptimal, and in some cases unstable,¹⁵ to run the open-loop reconstructors in closed loop.

In an effort to come to grips with these concepts, a very instructive simulation was run. For speed of implementation, a 2.5-m telescope was used. The guide star was a sodium LGS located at an elevation of 90 km. The tip-tilt information from the guide star was assumed to be valid. The turbulence was all located, and known to be located, at an elevation of 20 km (to exaggerate the effect of the conical sampling of the turbulence from the LGS), and it was corrected by a single DM conjugate to the ground. The WFs has *20times20* pixels to try to make the centroid response to wavefront slope as linear as possible.

Four cases were simulated:

1. Standard closed-loop control as used in classical LGS AO systems.
2. Open-loop control using the open-loop tomographic reconstructor.
3. Closed-loop control using the open-loop tomographic reconstructor.
4. Closed-loop control using the pseudo-open-loop tomographic reconstructor.

These four cases are summarized in Table 3, along with the results from the simulations. The poke matrices G_a and G_x (following the formalism of Ellerbroek and Vogel¹⁵) are created by using light from a source at 90 km and a DM at 0 and 20 km respectively. There are a few interesting findings from this simple experiment. The pseudo-

Case	Control	Residual wavefront	Strehl ratio
1	Closed-loop	$(G_a^T G_a + \alpha C_\phi^{-1})^{-1} G_a^T s$	0.771
2	Open-loop	$(G_x^T G_x + \alpha C_\phi^{-1})^{-1} G_x^T s$	0.816
3	Closed-loop	$(G_x^T G_x + \alpha C_\phi^{-1})^{-1} G_x^T s$	0.764
4	Closed-loop	$(G_x^T G_x + \alpha C_\phi^{-1})^{-1} G_x^T s + (G_x^T G_x + \alpha C_\phi^{-1})^{-1} (G_x^T (G_a - G_x) - C_\phi^{-1}) a$	0.872

Table 3: Summary of the four cases simulated for LTAO toy problem.

open loop control method (Case 4) outperforms all the others, because it combines a tomographic reconstruction (optimal estimation) with closed-loop operation (mitigates non-linear effects of wavefront sensing). This method will be used in the simulations of the LTAO system for GMT. Running the tomographic reconstructor in a standard control loop (Case 3) produces a stable system in this case: however, if an SVD reconstructor based on the G_x matrix is used instead, the loop is unstable, leading us to believe that the regularization stabilizes the loop at a cost in performance. Ellerbroek and Vogel were unable to find a regularization term to stabilize the loop for the MCAO system they simulated:¹⁵ this could be due to either the increased complexity of the system they were trying to model or the fact that their regularization term was less aggressive at forcing a smooth reconstructed wavefront.

4. RESULTS

While the simulation effort is still in its infancy, some of interesting results, presented in this section, have already been gleaned by this work.

4.1 Atmospheric segment piston error

One area of concern for the GMT is the atmospheric component of the piston segment error. This is the error in the reconstruction when only the wavefront slopes are known, with no additional information about how the segments are phased. Note that the regularized least-squares reconstructor was used, and this forces the wavefront to be as smooth as possible; hence the piston segment error comes about because the true wavefront is not as smooth between the segments as it could be due to high spatial frequency components. We are also interested in knowing the frame rate at which a piston sensor would need to run in order to compensate for this error.

We used an ideal piston sensor and a piston DM, described in Section 2.2. YAO allows the use of different integration times for different control loops provided that they are integer multiples of the main control loop.

The simulation was run at a frame rate of 1000 Hz, with a single atmospheric layer with r_0 of 0.2 m traveling at 10 ms^{-1} . The average K-band Strehl ratio was 0.840 and 0.722 for simulations with and without the piston WFS. Using the Maréchal approximation, this corresponds to a segment piston error of 136 nm. The residual segment piston error, as measured by the piston WFS, is tabulated in Table 4. The segment piston error has been calculated using semi-analytic methods to be $35r_0^{-5/6}$ nm, or 134 nm for a Fried parameter of 20 cm, which agrees extremely well with the number found in the simulations. The temporal power spectrum of the

Piston WFS frame rate (Hz)	1000	250	100	40	0
Uncorrected segment piston RMS error (nm)	9	34	99	120	126

Table 4: Atmospheric segment piston error as a function of frame rate in the piston wavefront sensor loop.

uncorrected segment piston error obtained from the simulations is plotted in Figure 1. The segment piston has a large high temporal frequency component and must be corrected at frame rates commensurate with that of the WFS or even higher. Slow methods for measuring segment piston might be applicable to removing the telescope contribution, but not the atmospheric contribution, to segment piston.

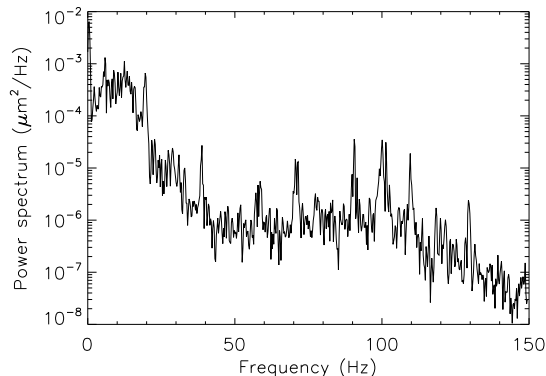


Figure 1: Temporal power spectrum of the uncorrected segment piston error.

4.2 Comparison of atmospheric turbulence generation

A key component of any AO simulation package is an atmospheric turbulence generator. It is important to use phase screens with the right statistics in order to obtain consistency between one simulation tool to another and to accurately predict what will happen on the sky. Many different techniques have been proposed in the literature and implemented in publicly available code. The high and low spatial frequencies are both very important. The high spatial frequencies comprise the bulk of the error terms in classical on-axis NGS AO systems: fitting error, aliasing error, bandwidth error and reconstruction error. The low spatial frequencies are very important for tip-tilt errors and anisoplanatic errors, both of which can dominate the error budget when using LGSs as beacons.

There are two broad brush approaches to generating phase screens: either using piston-removed covariance matrices to produce screens with the right covariance or by Fourier filtering a power spectrum to produce screens with the right power spectrum.

All of the Fourier based methods suffer from a reduction in low spatial frequencies. This is a well known phenomenon, and can be mitigated by one of the following two techniques:

- Generate a phase screen much larger than the pupil and use a small section of the phase screen.
- Generate subharmonics of the phase power spectrum to incorporate the lower spatial frequencies

In what follows, we compare the statistics of the phase screens produced by a number of different codes. For each method, 100 512x512 screens were generated and used to compute the statistics and these are compared to the theoretical values in Noll.¹⁶

Phase covariance: Calculate the piston-removed covariance between points on the phase screen using the method of Wallner.¹⁷ A fast implementation in Matlab that uses mid-point displacements to produce large phase screens developed by Harding *et al* was used.¹⁸

Fourier filtering: Generate random numbers with Gaussian statistics and filter in the Fourier domain with the appropriate power spectrum. The code in YAO, written in Yorick, was used. It is known that there is an implicit outer scale of about half the phase screen due to the periodicity of the phase screens. Therefore, this method was not expected to produce phase screens with the correct statistics at low spatial frequencies.

Fourier filtering (subsection): Generate 4096x4096 phase screens using the Fourier filtering method and extract 512x512 subsections.

Fourier filtering with subharmonics: Generate phase screens using Fourier filtering and adding subharmonics to compensate for the lack of low spatial frequency power. An IDL implementation of the the method of Johansson and Gavel¹⁹ was used, with the number of subharmonic levels set to eight.

Table 5 tabulates the power in the piston-removed phase screen as well as the low-order Zernike coefficients for a number of different methods. It can be seen that several of the methods underestimate the amount of tip-tilt. In addition, the Fourier-based methods produce phase screens are not isotropic at low frequencies; an inspection of Table 5 shows that there is a lot more power in Z_6 (zero-degree astigmatism) compared to Z_5 (45-degree astigmatism). This situation does not change by adding subharmonics, but is improved by taking a section of the phase screen.

Method	Total power	Z_2	Z_3	Z_4	Z_5	Z_6
Theoretical	1.030	0.448	0.448	0.023	0.023	0.023
Covariance	0.978	0.464	0.381	0.025	0.025	0.021
Fourier filtering	0.185	0.022	0.022	0.021	0.009	0.031
Fourier filtering (subsection)	0.932	0.336	0.426	0.028	0.037	0.034
Fourier filtering with subharmonics	0.774	0.358	0.282	0.025	0.010	0.034

Table 5: Comparing the total power and the power in the Noll Zernike modes for a variety of phase screen simulation tools.

To test for the correctness of the statistics of the phase screens, we also compared the structure functions of the phase screens against the theoretical values. The phase structure function is defined as

$$D_\phi(x) = E[(\phi(x+x') - \phi(x'))^2], \quad (5)$$

where $\phi(x)$ is the phase at location x and $E[\cdot]$ denotes the expectation operator. For Kolmogorov turbulence, it is given by:

$$D_\phi(x) = 6.88(x/r_0)^{5/3}. \quad (6)$$

The phase structure function was computed directly by shifting the phase screens in x and in y , and averaging the results. Figure 2 compares the structure function of these methods with the theoretical curve. It shows that if we do not use a phase covariance based method, we must ensure that the phase screen generated is much larger than the region of interest. Adding subharmonics helps to improve the match between the structure function and the theoretical curve.

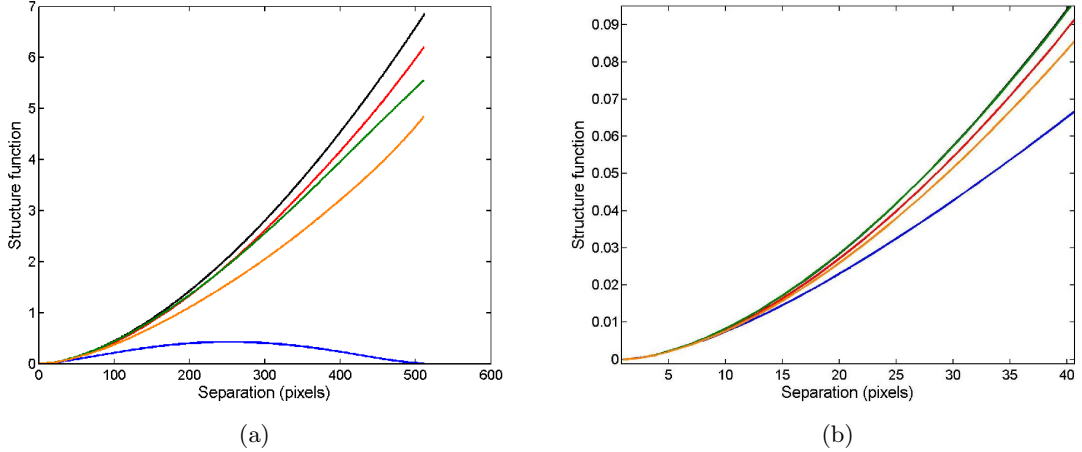


Figure 2: Structure functions for (a) from top to bottom are: theory, covariance, Fourier filtering subsection, Fourier filtering with and without subharmonics. For (b), they are: theory, Fourier filtering subsection (almost coincident), covariance, Fourier filtering with and without subharmonics. Graph (a) shows the whole curve, while (b) zooms in near the origin (corresponding to the high spatial frequencies.)

A modification to the Kolmogorov power spectrum that is commonly made is to use the von Karman power spectrum, which incorporates a turbulence outer scale, L_0 . Phase screens were generated using Fourier filtering with subharmonics and the results are tabulated in Table 6 and compared with the theoretical results were calculated according to an evaluation of the formulas in Winker.²⁰ The Harding *et al* implementation of the phase covariance method does not support outer scales.

Method	L_0/D	Z_2	Z_3	Z_4	Z_5	Z_6
Theoretical	∞	0.426	0.426	0.0232	0.0232	0.0232
Simulations	∞	0.358	0.282	0.0250	0.0100	0.0340
Theoretical	4	0.082	0.082	0.0175	0.0175	0.0175
Simulations	4	0.0677	0.0788	0.0199	0.0085	0.0256
Theoretical	2	0.0343	0.0343	0.0113	0.0113	0.0113
Simulations	2	0.0284	0.0319	0.0141	0.0070	0.0199
Theoretical	1	0.0088	0.0088	0.0045	0.0045	0.0045
Simulations	1	0.0076	0.0084	0.0051	0.0028	0.0061

Table 6: Comparing the theoretical power in the Noll Zernike modes with simulation results using the Fourier filtering with subharmonics method for a variety of von Karman outer scale values.

5. CONCLUSION

The aim of this study was to determine whether YAO, a general-purpose AO simulation tool written in Yorick, is applicable to the GMT modeling effort. We have found that, with some modifications to the code, it is possible to run useful simulations for the NGS AO and GLAO cases. The simulations run sufficiently quickly that they can be carried out on a standard computer. We are in the process of extending the capabilities of YAO to run

LTAO simulations using the pseudo open-loop control method. In the future, we also hope to be able to use YAO to compare the pyramid WFS with the Shack-Hartmann WFS in NGS AO mode and also to determine the benefits of sharpening the tip-tilt guide star in LTAO.

The segment piston error is a significant and high spatial and temporal frequency error term for the GMT and ways to mitigate this are needed.

A comparison of different turbulence generation methods shows that they are not all created equal. While it is known that Fourier filtering produces phase screens with too little power at low spatial frequencies, it is not always practical to create phase screens that are eight times longer and wider. Using the subharmonic method mitigates this problem, but the resulting phase screens still have three times as much power in the 90-degree astigmatism mode relative to 45-degree astigmatism.

ACKNOWLEDGMENTS

Thanks are due to Miska Le Louarn for useful advice on running AO simulations.

This Work is being supported through a sub-award to CIW from the Association of Universities for Research in Astronomy Inc. (AURA) from funds provided by the National Science Foundation under the Scientific Program Order No. 10 as issued for support of the Giant Segmented Mirror Telescope for the United States Astronomical Community, in accordance with Proposal No. AST-0443999 submitted by AURA.

REFERENCES

- [1] M. Le Louarn *et al*, "Progress and prospects in adaptive optics simulation capabilities," Proc. SPIE **7736** (2010).
- [2] P. M. Hinz *et al*, "The GMT adaptive optics system," Proc. SPIE **7736** (2010).
- [3] R. P. Knox *et al*, "Modeling adaptive optics for the segmented aperture of the GMT," Proc. SPIE **7736** (2010).
- [4] <http://www.maumae.net/yao/>
- [5] M. A. van Dam, D. Le Mignant and B. A. Macintosh, "Performance of the Keck Observatory Adaptive-Optics System," Appl. Opt. **43**, 5458-5467 (2004).
- [6] D. Gavel, "Suppressing anomalous localized waffle behavior in least squares wavefront reconstructors," Proc. SPIE **4839**, 972-980 (2003).
- [7] B. L. Ellerbroek, "Efficient computation of minimum-variance wave-front reconstructors with sparse matrix techniques," J. Opt. Soc. Am. A **19**, 1803-1816 (2002).
- [8] <http://homepage.mac.com/rflicker/soy.htm>
- [9] D.T. Gavel *et al*, "Visible light laser guidestar experimental system (Villages): on-sky tests of new technologies for visible wavelength all-sky coverage adaptive optics systems," Proc. SPIE **7015**, 70150G (2008).
- [10] R. M. Clare, M. A. van Dam and A. H. Bouchez, "Modeling low order aberrations in laser guide star adaptive optics systems," Opt. Express **15**, 4711-4725 (2007).
- [11] A. Tokovinin, "Seeing Improvement with GroundLayer Adaptive Optics, PASP **116**, 941951 (2004)
- [12] M. Le Louarn and N. Hubin, "Improving the seeing with wide-field adaptive optics in the near-infrared. Monthly Notices of the Royal Astronomical Society **365**, 1324-1332 (2005).
- [13] T. Fusco, J.-M. Conan, G. Rousset, L. M. Mugnier, and V. Michau, Optimal wave-front reconstruction strategies for multi-conjugate adaptive optics, J. Opt. Soc. Am. A **18**, 25272538 (2001).
- [14] D. T. Gavel, "Tomography for multiconjugate adaptive optics systems using laser guide stars," Proc. SPIE **5490**, 1356 (2004)
- [15] B. L. Ellerbroek and C. R. Vogel, "Simulations of closed-loop wavefront reconstruction for multiconjugate adaptive optics on giant telescopes," Proc. SPIE **5169**, 206 (2003).
- [16] R. J. Noll, "Zernike polynomials and atmospheric turbulence," J. Opt. Soc. Am. **66**, 207-211 (1976).
- [17] E. P. Wallner, "Optimal wave-front correction using slope measurements," J. Opt. Soc. Am. **73**, 1771-1776 (1983).

- [18] C. M. Harding, R. A. Johnston, and R. G. Lane, "Fast Simulation of a Kolmogorov Phase Screen," *Appl. Opt.* **38**, 2161-2170 (1999).
- [19] E. M. Johansson and D. T. Gavel, "Simulation of stellar speckle imaging," *Proc. SPIE* **2200**, 372 (1994).
- [20] D. M. Winker, "Effect of a finite outer scale on the Zernike decomposition of atmospheric optical turbulence," *J. Opt. Soc. Am. A* **8**, 1568-1573 (1991).